Fabrication and characterization of microfabricated on-chip microelectrochemical cell for biosensing applications

N. A. Mohd Said, K. Twomey, G. Herzog, and V. I. Ogurtsov

Citation: AIP Conference Proceedings **1808**, 020032 (2017); doi: 10.1063/1.4975265
View online: http://dx.doi.org/10.1063/1.4975265
View Table of Contents: http://aip.scitation.org/toc/apc/1808/1
Published by the American Institute of Physics

Fabrication and Characterization of Microfabricated on-chip Microelectrochemical Cell for Biosensing Applications

N. A. Mohd Said,[1,2] K. Twomey,[1] G. Herzog[3] and V.I. Ogurtsov,[1, a)]

[1]*Tyndall National Institute, University College Cork, Lee Maltings Prospect Row, Cork, Republic of Ireland*
[2]*Current affiliation: Biotechnology Research Centre, Malaysian Agricultural Research and Development Institute (MARDI), P.O Box 12301, General Post Office, 50774 Kuala Lumpur, Malaysia*
[3]*LCPME, UMR 7564, CNRS-Université de Lorraine, 405, Rue de Vandœuvre, 54600, Villers-lès-Nancy, France*

[a)]Corresponding author: vladimir.ogourtsov@tyndall.ie

Abstract. The fabrication of on-chip microelectrochemical cell on Si wafer by means of photolithography is described here. The single on-chip microelectrochemical cell device has dimensions of 100 x 380 mm with integrated Pt counter electrode (CE), Ag/AgCl reference electrode (RE) and gold microelectrode array of 500 nm recess depth as the working electrode (WE). Two geometries of electrode array were implemented, band and disc, with fixed diameter/width of 10 μm; and varied centre-to-centre spacing (*d*) and number of electrodes (*N*) in the array. The on-chip microelectrochemical cell structure has been designed to facilitate further WE biomodifications. Firstly, the developed microelectrochemical cell does not require packaging hence reducing the production cost and time. Secondly, the working electrode (WE) on the microelectrochemical cell is positioned towards the end of the chip enabling modification of the working electrode surface to be carried out for surface bio-functionalisation without affecting both the RE and CE surface conditions. The developed on-chip microelectrochemical cell was examined with scanning electron microscopy (SEM) and characterised by two electrochemical techniques. Both cyclic voltammetry (CV) and electrochemical impedance spectroscopy (EIS) were performed in 1 mM ferrocenecarboxylic acid (FCA) in 0.01 M phosphate buffered saline (PBS) solution at pH7.4. Electrochemical experiments showed that in the case of halving the interspacing distance of the microdisc WE array (50 nm instead of 100 nm), the voltammogram shifted from a steady-state CV (feature of hemispherical diffusion) to an inclined peak-shaped CV (feature of linear diffusion) albeit the arrays had the same surface area. In terms of EIS it was also found that linear diffusion dominates the surface instead of hemispherical diffusion once the interspacing distance was reduced, supporting the fact that closely packed arrays may behave like a macroelectrode

INTRODUCTION

One of the ultimate objectives in biosensor development is its viability to carry out the analysis at the point of need i.e. outside the laboratory. This necessitates the miniaturization, as well as the portability, of the whole biosensor system. With regard to the biosensor measurement, electrochemical biosensors are still favoured over the other biosensor approaches (optical, mass etc.) owing to their stability and simple label-free operation procedure that eliminates sample pre-treatment. In order to achieve miniaturization and to complement the handhold-sized electrochemical analyser/potentiostats, which are commercially available in market, the fabrication of three-cell electrodes (RE, CE and microarray WE) integrated on a single chip (hereafter referred as 'on-chip microelectrochemical cell') is of paramount importance.

Microelectrode arrays offer a number of advantages which include: improved mass transport and increased sensitivity (due to hemispherical diffusion), steady or quasi-steady state responses for Faradaic processes, reduced ohmic (iR) drop and most importantly for sensing applications, improved signal-to-noise ratios allowing lower detection levels if to compare with a sensor based on macro size electrodes [1]. Thus, microfabricated electrochemical sensors with WE microelectrode array can provide sufficient sensitivity and achieve limits of detection required for practical applications [2].

11th Asian Conference on Chemical Sensors
AIP Conf. Proc. 1808, 020032-1–020032-13; doi: 10.1063/1.4975265
Published by AIP Publishing. 978-0-7354-1476-1/$30.00

The successful fabrications of on-chip microelectrochemical cell and their application in variety fields have been reported by several research teams over the past few years. These include silicon chips for robotic fish used for the detection of pollutants in seawater [2,3], screen-printed microelectrode arrays for the detection of chromium (VI) in environmental (canal water) [4], needle-type microelectrode for simultaneous detection of nitrite and dissolved oxygen [5], microfabricated immunochip for aflatoxin M1 detection [6], wearable screen-printed electrode for visual indication on water quality (environmental pollutants) and security threats in marine environments [7] and an electronic tongue for tasting the freshness of milk [8].

Here, we report the development, fabrication and characterization on-chip microelectrochemical cell which consists of Ag/AgCl reference electrode (RE), Pt auxiliary/counter electrode (CE) and an array of microdisc or microband gold working electrodes. The cell is located on a chip with dimension of 100 mm x 380 mm (Fig. 1a). The device also includes contact pads with associating tracks that connect pads to the corresponding electrodes. The pads were arranged in such a way that chip could be connected to the instrumentation by sliding the transducer pads into an appropriate connector. This on-chip microelectrochemical cell was designed with consideration of several aspects important for further applications after the electrode fabrication. Firstly, unlike most of lab-on-chip/chip-on-board/biochips which require an additional separate integration process to assemble the different parts of the electrodes [3,9], the developed microelectrochemical cell is ready immediately after wafer dicing (Fig. 1b) as it does not require packaging hence reducing the sensor production cost and time. This microelectrochemical cell can be used straight away in the next step of biofunctionalisation after the fabrication with simple post production electrode surface treatment (e.g. oxygen plasma) without the risk of epoxy contamination that derived from the packaging step. Secondly, the working electrode (WE) on the microelectrochemical cell is located at the end of the chip. Such arrangement comes in handy during surface bio-functionalisation step whereby the modification of WE surface will not interfere and affect both RE and CE surface as opposed to electrodes that are designed adjacently to each other.

In this study, the fabricated on-chip microelectrochemical cells have two different geometries of WE, namely microdisc and microband array. Each geometry designs have a fixed dimension of 10 μm diameter (microdisc) or 10 μm width (microband) with different centre-to-centre distance (d) (d=100 μm and 50 μm) and different number of electrodes in the array (N) (Table 1 and 2). All disc array designs were arranged in hexagonal configuration instead of cubic one as this arrangement provides more space-saving placement of the discs on the available WE area. In total, 12 types of on-chip microelectrohemical cell were designed, fabricated and characterized. This miniaturized device will lend itself well in providing a straight-forward application following fabrication as well as a portable sensor platform that allows miniaturization of biosensor for in-situ measurements.

TABLE 1 Geometrical parameters of on-chip microelectrochemical cells with disc array (denote as D)

	Design	Geometry	Diameter (μm)	*d*, Spacing (centre-to-centre) (μm)	*N*, number of electrodes	Surface area (cm^2)
	D1			100	314	2.466×10^{-4}
Wafer 1	D2			100	150	1.178×10^{-4}
	D3	Disc	10	100	86	6.755×10^{-5}
	D4			50	314	2.466×10^{-4}
Wafer 3	D5			50	150	1.178×10^{-4}
	D6			50	86	6.755×10^{-5}

TABLE 2 Geometrical parameters of on-chip microelectrochemical cells with band array (denote as B)

	Design	Geometry	Width (μm) x length (μm)	*d*, Spacing (centre-to-centre) (μm)	*N*, number of electrodes	Surface area (cm^2)
	B1			100	18	9.0×10^{-4}
Wafer 2	B2			100	9	4.5×10^{-4}
	B3	Band	10x500	100	5	2.5×10^{-4}
	B4			50	18	9.0×10^{-4}
Wafer 4	B5			50	9	4.5×10^{-4}
	B6			50	5	2.5×10^{-4}

MATERIALS AND METHODS

On-chip Microelectrochemical Cell Fabrication

Schematic diagrams depicting the fabrication process for each part of the microelectrochemical cell are presented in Fig. 1c. The electrodes on the on-chip microelectrochemical cell were pre-patterned on a Si substrate and fabricated by standard photolithography and lift-off techniques. For WE fabrication, the process was as described elsewhere [10]. Additional fabrication process entailing the CE and RE are described here. It included Pt e-beam evaporation for the CE construction. Titanium was used in the proportion of 20:100 Ti:Pt to ensure appropriate adhesion of the Pt layer to the silicon. After metal evaporation, the excess metal and photoresist were lifted off in R1165 resist stripper. The Ti:Ni:Ag layer (20:50:250) was only evaporated after the passivation etch as etch chemistry would damage the Ag layer. The Ag electrodes were then treated with $FeCl_3$ [11] followed by the lift-off technique. Following fabrication, the on-chip electrochemical cells wafers were diced and no further electrodes packaging were required. All microfabrication processing was carried out at the Central Fabrication Facility at Tyndall National Institute, Cork, Ireland.

SEM Imaging and EDX Analysis

The fabricated on-chip microelectrochemical cells were inspected using scanning electron microscopy (SEM) (Quanta 650 FEG, Oregon USA) to verify the dimensions of the array geometries, including the recess depth. The energy-dispersive X-ray spectroscopy (EDX) analysis was utilised to confirm the presence of gold, silver and platinum layers on the working, reference and counter electrodes respectively.

Electrochemical Measurements

All electrochemical characterisations (CV and EIS) were carried out in 0.1 M ferrocenecarboxylic acid in PBS (pH 7.4); both chemicals were from Sigma-Aldrich Ireland Ltd. A customised connector was used to hold the on-chip microelectrochemical cell. The on-chip microelectrochemical cell was plasma cleaned (Harrick Plasma USA) for 10 minutes first prior electrochemical measurements. Electrochemical experiments were done using a potentiostat PGSTAT 302N from Ecochemie (Metrohm, United Kingdom). In a comparison study, commercial reference electrode of Ag|AgCl|1 M KCl and counter electrode of Pt wire were used.

RESULTS AND DISCUSSIONS

Visual Examination

From the SEM images, microdisc arrays were confirmed to have diameter of 10 μm. The recess depth was found to be an approximate of between 400-720 nm, deviation of 20-44% from the expected 500 nm recess depth. The distance between discs were found to be in the vicinity of 86 μm and 37 μm which will made up the disc centre-to-centre spacing approximated to 96 μm for the 100 μm spacing and 47 μm for the 50 μm spacing respectively (Fig. 2).

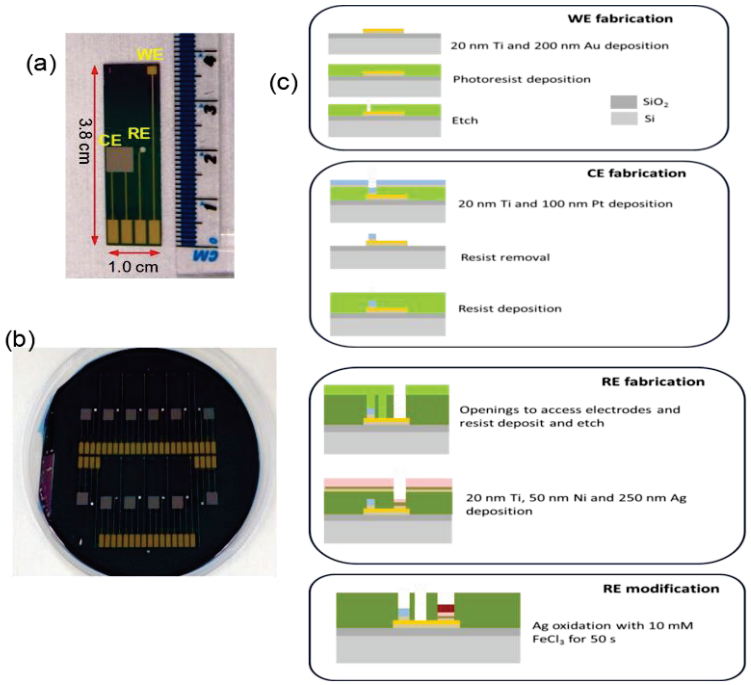

FIGURE 1. (a) Single on-chip microelectrochemical cell; (b) Silicon wafer containing fabricated on-chip microelectrochemical cells; and (c) Schematic diagram of fabrication process for different parts (WE, CE and RE) of the on-chip microelectrochemical cell

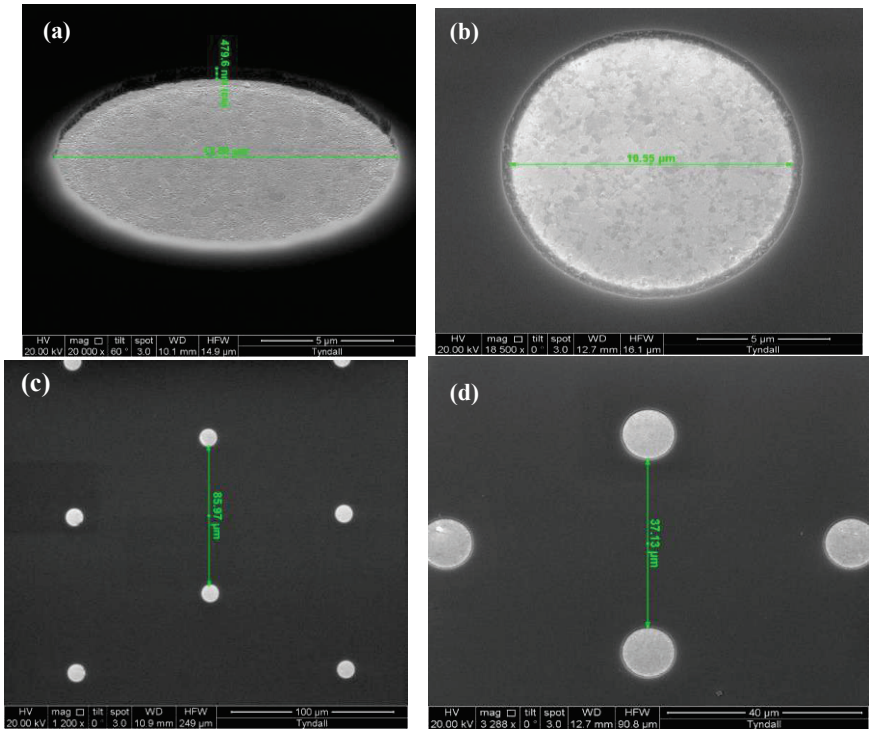

FIGURE 2. SEM images for on-chip microelectrochemical cell with disc arrays. (a,b) Disc's diameter and recess measurements; and centre-to-centre distance (*d*) expected for (c) 100 µm spacing; and (d) 50 µm spacing

For the microband array, the achieved dimensions for the fabricated electrodes were in better agreement with the dimensions expected. The band lengths were confirmed to have 493.5 nm which is close to 500 nm as expected. The width of the band was found to be 11.51 µm on tilted position with the range of 600 nm recess depth (Fig. 3).

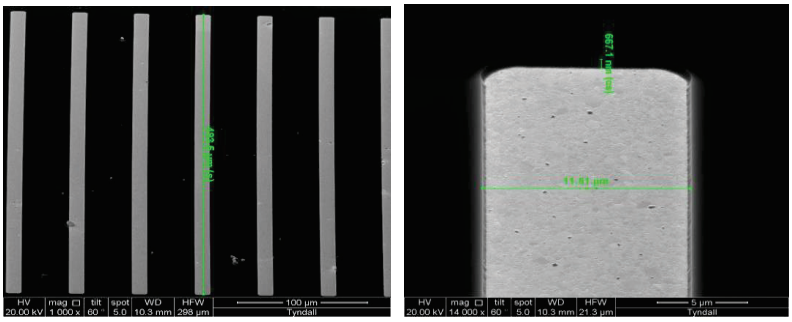

FIGURE 3. SEM images for on-chip microelectrochemical cell with band arrays.

The EDX analysis confirmed the presence of gold for the WE surface, silver for RE surface and platinum for CE surface (Fig. 4). However there was no chloride detected in the RE component, suggesting the instability of the Cl layer formed on the electrode after the Cl treatment. The Cl counterpart might have been peeled off during the lift-off process in fabrication or after several electrochemical measurements. Ti element was presented in all the spectra as it was used to adhere the electrode metals to the silicon substrate. The presence of Ni on the RE surface may suggest that some amount of Ni was used as well to adhere Ag metal to the silicon besides Ti as for pyrex/silicon substrate [12]. Some traces of Fe, C, N and K were also found in the RE EDX spectra, which could be derived from the potassium hexaferricyanide solution in sodium chloride used to do some electrochemical measurements of the on-chip microelectrochemical cell prior the SEM/EDX analysis.

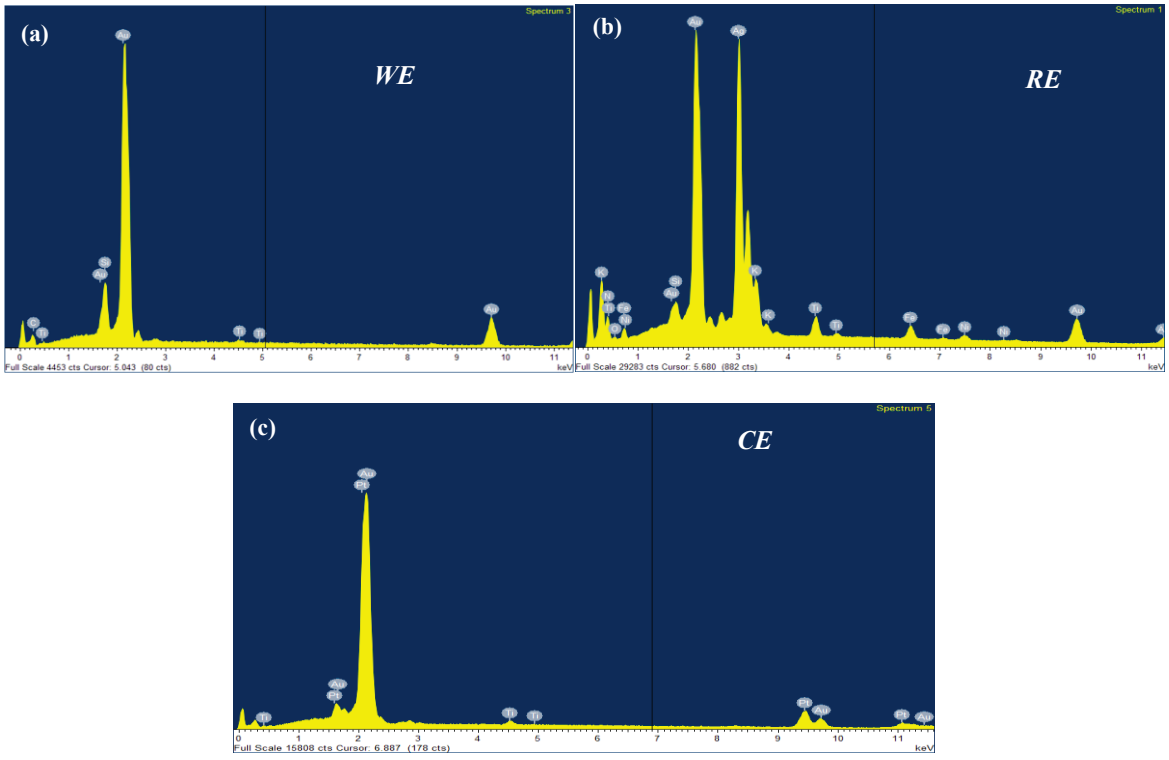

FIGURE 4. EDX spectrum of the (a) Au microelectrode array; (b) Ag reference electrode; and (c) Pt counter electrode

Electrochemical Characterisations

Characterisation of on-chip Electrodes and Commercial Electrodes

The electrochemical performance of the fabricated on-chip Ag reference electrode and Pt counter electrode were first evaluated by comparing the CVs taken from the on-chip cell as a one-piece device (hereafter referred as *on-chip* measurement/reading); and WE from the chip with external commercial Ag/AgCl and Pt wire electrodes (hereafter referred as *off-chip* measurements/reading). Four modes of measurements were performed: (i) all-on-chip reading (using both RE and CE on the on-chip microelectrochemical cell); (ii) CE commercial (RE on-chip); (iii) RE commercial (CE on-chip); and (iv) both RE and CE commercial. The voltammograms were obtained in 3 repetitions at a scan rate of 100 mV s^{-1}. As shown in Fig. 5, the voltammograms displayed identical peak shapes and currents, but different peak potentials, which can be attributed to the reference electrodes properties [3]. Moreover, all voltammograms were obtained with good reproducibility, stability, and reversibility, indicating the successful operability of the fabricated Ag/AgCl reference electrode and platinum counter electrode.

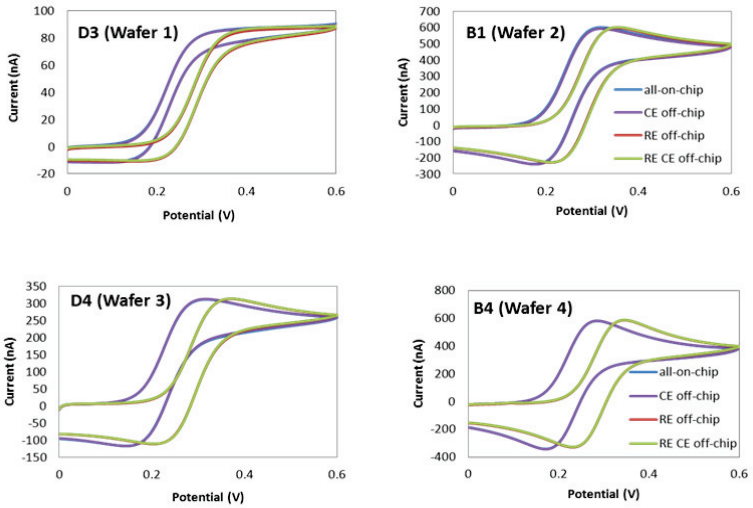

FIGURE 5. On-chip measurements for fabricated microelectrochemical cells (one design from each wafer) compared with readings from commercial RE and CE in 1 mM FCA in PBS, scan rate of 100 mV s^{-1}.

Similar results for the peak shift using commercial Ag/AgCl reference electrode in comparison with on-chip RE were also reported before by Moujahid et al. (2011) [3] and Chen et al. (2000) [13]. In both cases, the RE layer on-chip was retreated with silver and chloride ion oxidised in either HCl or KCl to form AgCl layer. In our study, the formation of AgCl composition was carried out after the deposition of Ti:Ni:Ag layer by submerging the wafers in the $FeCl_3$ solution for 50 seconds as described by Polk et al. (2006) [11]. The shift of the electrode potentials was due to difference of chloride concentrations. The potential difference between the on-chip and commercial RE can be determined according to the Nernst equation:

$$E_{Ag\,|AgCl} = E^{0}_{Ag\,|AgCl} + \frac{RT}{nF} ln\, a_{Cl^-} \tag{1}$$

where $E_{Ag|AgCl}$ is the standard potential for the Ag/AgCl electrode ($E_{Ag|AgCl}$ is 0.2223) and a_{Cl^-} is the chloride activity which can be approximated to the chloride concentration in the solution.

The results obtained for the expected potential according to the equation were 0.1467 V for the chloride in 1 mM FCA in PBS and 0.2223 V for the chloride in 1M potassium chloride. The potential on the on-chip RE measurements were found 0.1531 ± 0.014 V, which were close with the calculated ones.

Limiting Current and Cyclic Voltammetry Study

The experimental limiting current, i_{lim}, for the different microelectrochemical cell designs were obtained by averaging three readings or more from one or more measurements (Table 3). All measurements were taken using all-on-chip electrochemical readings. The values were then compared with theoretical current by employing Equation 2 for microdisc array [14] and Equation 3 for microband array [15].

$$i_{lim} = \left(\frac{4\pi nFCDr^2}{4L + \pi r}\right)N \tag{2}$$

$$i_{lim} = \frac{nFDCl}{\left(\frac{1}{2\pi}\ln\left(\frac{64Dt}{w^2}\right) + \frac{L}{w}\right)}N \tag{3}$$

In these equations n is the number of electrons involved in the reaction, F is Faraday constant (96,485 C mol^{-1}), C is the bulk concentration of ferrocene carboxylic acid (mol cm^{-3}), D is diffusion coefficient (5.7×10^{-6} cm^2 s^{-1}), r is the disc radius (cm), L is the silicon nitride thickness (recess depth) (cm), N is the number of electrodes in an array, l is the band electrode length (cm) and w is the band electrode width (cm).

TABLE 3. Comparison between the theoretical current and experimental current for microelectrode array working electrode for on-chip electrochemical cell

Design	Recess depth (nm)	Theoretical current, nA	Experimental current, nA
D1	715	292	301.8 ± 26.01
D2	748	139	160.3 ± 3.42
D3	660	81	80.7 ± 6.42
D4	778	288	268. 6 ± 7.28
D5	479	147	156.1 ± 2.73
D6	612	79.9	119.4 ± 2.56
B1	765	622	550 ± 9.75
B2	675	314	223.3 ± 17.75
B3	n/a	173	151.3 ± 0.64
B4	681	628	500.9 ± 28.3
B5	667	315	218.7 ± 9.15
B6	656	175	142.5 ± 28.88

For the first three disc designs with interspacing distance of 100 μm (D1-D3), sigmoidal shape CVs were observed indicating the occurence of hemispherical diffusion of the ferrocenecarboxylic acid towards the microdiscs with non-overlapping diffusion zones between the neighboring microdiscs. This is validated by the experimental limiting currents achieved for those designs which are relatively close with the theoretical currents. With decreasing number

of disc array (N=86) and insufficient interspacing distance between the discs (50 µm instead of 100 µm) the sigmoidal shape of the CV is shifted to a peak-shaped CV (Fig.6) demonstrating that the planar or mixed diffusion (individual with overlapping diffusion profile); has taken over the hemispherical diffusion [16]. The experimental limiting currents increased linearly with the number of microdiscs in the array with a determination coefficient r^2=0.9923 and r^2=0.9986 for d of 100 and 50 µm respectively (Fig. 7).

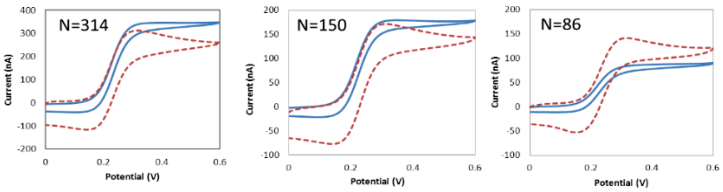

FIGURE 6. The diminishing sigmoidal signal as distance between the disc's interspacing was reduced from d=100 µm (blue line) to d=50 µm (red dotted line). Scan rate 100 mV s^{-1} in 1mM FCA in PBS.

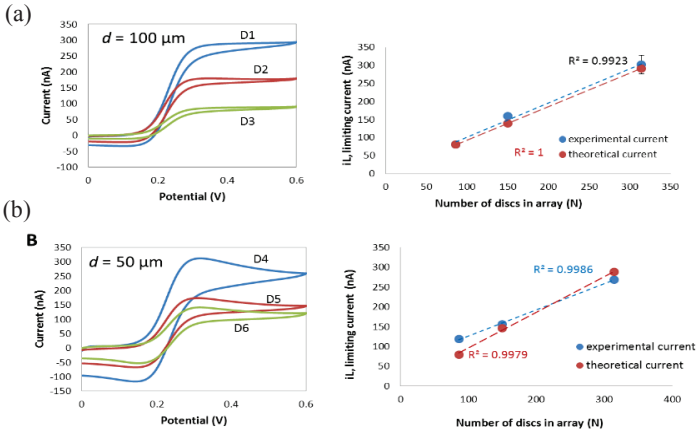

FIGURE 7. Cyclic voltammetry for disc microelectrode array fabricated on microelectrochemical cell (a) D1-D3; and (b) D4-D6. Measurements were carried out using on-chip electrochemical cell with scan rate of 100 mV s^{-1} in 1mM FCA in PBS. *Insets*: i_{lim} as a function of N for both experimental (blue marker) and theoretical currents (red marker).

For a microelectrochemical cell with the microband array, the theoretical limiting current exceeded the experimental values with discrepancy between current values in the range of 11-31%. The diffusion profile suggested for the fabricated band array was a mixed diffusion profile hence this can be accounted for the large difference between the current values. The voltammogram shapes obtained for the band interspacing centre at 100 µm (B1-B3) showed typical quasi-steady state voltammograms as reported for microband array [17]. This voltammogram however has shifted to a more pronounced peak-shaped CV when the interspacing was reduced by half to 50 µm for B4-B6 (Fig. 8). This effect was clearly obvious when the number of array has greatly decreased (N=5). The diffusion profile that would be suggested for the B6 is a planar diffusion, which happens when insufficient spacing is designed on an electrode array [18]. Comparing the CV for B4-B6, the B6 design has similarity with previous reported D6 where their experimental currents deviate significantly from the theoretical current indicating overlapping/planar diffusion that has taken place in the system.

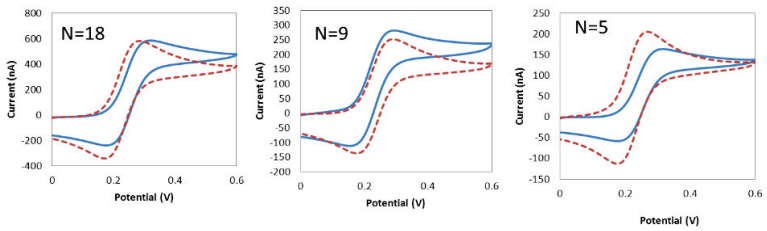

FIGURE 8. The voltammogram for microband array microelectrochemical cells shifted to a peak-shaped CV when band spacing distance was reduced from 100 μm (blue line) to 50 μm (red dotted line). Scan rate100 mV s^{-1} in 1 mM FCA in PBS.

To conclude all the fabricated on-chip microelectrochemical cells for the limiting current study, the correlation between theoretical and experimental current for all designs were presented in Fig. 9. The correlation gave a good r^2 value of 0.9508 considering the fact that irregularity in the recess depth fabricated was noted.

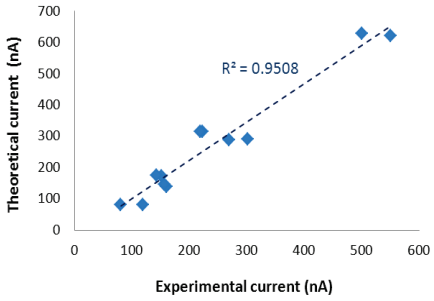

FIGURE 9. Correlation between experimental and theoretical current for all fabricated on-chip microelectrochemical cell.

For the following study, it was found that several designs of microelectrode array electrodes were no longer active. Microscopic images below compares two microdisc designs of D2 and D3; where D2 consisted of dead electrodes whilst all the electrodes in D3 are active. The presence of active electrodes could be indicated by the gold layer which seen underneath the microdiscs. On the other hand, if the electrodes are dead, black dots were observed representing the absence of gold. Lithographic fabrication procedures used are known to be associated with the presence of dead or inactive electrodes which eventually lead to a lower limiting current [2, 19, 20]. For the microband electrode of B3, it is also observed that no gold layer left within the recess surface after several usages. In comparison, an active microband would have a layer of gold presence. We could attribute this to the lamination of the band electrode. Lamination is one of the defect or failure mode that normally occurs in silicon based microsensors [21, 22]. As have been reported, non-uniform current densities on the electrode surface can contribute on electrodes damage [23, 24].

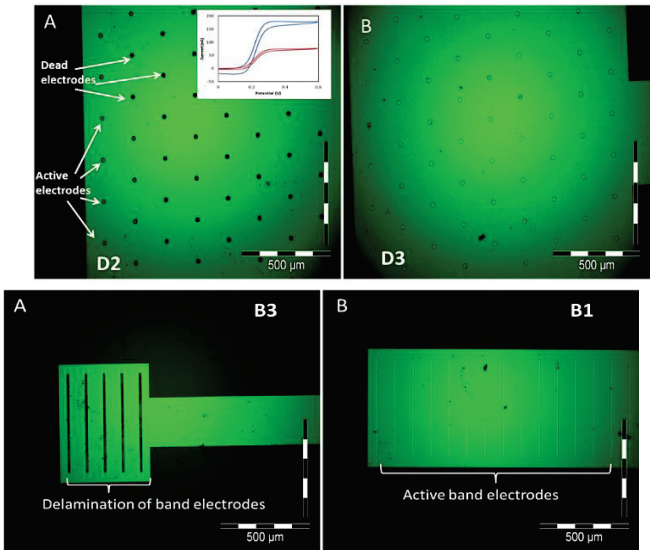

FIGURE 10. Top Row: Microscopic images of dead discs on design D2 (N=150, d=100 µm), represented by black dots (*inset*: current depletion voltammogram before (blue line) and after (red line) dead electrode occurance); and active disc electrodes on D3 (N=86, d=100 µm) with gold layer underneath the discs. Magnification 20x. Bottom row: Delamination of gold microband array in B3 (N=5, d=100 µm) and active microband with gold layer for design B1 (N=18, d=100 µm). Magnification 10x.

Electrochemical Impedance Spectroscopy (EIS) Study

A comparative EIS study between all-on-chip electrodes with off-chip (commercial) RE and CE was carried out in order to ensure that all on-chip EIS measurements are reliable. The average reading was taken to draw the respective Nyquist plot. Both EIS curves using on-chip RE and CE were comparable with commercial electrodes measurements (Fig. 11) where overlapping of diffusion zones seemed to occur at frequency below of 0.119 Hz. The similarity exhibited between these two modes of measurement proved the reliability of the microfabricated RE and CE and thus allowed us to characterise the remaining microelectrochemical cells using all-on-chip measurements.

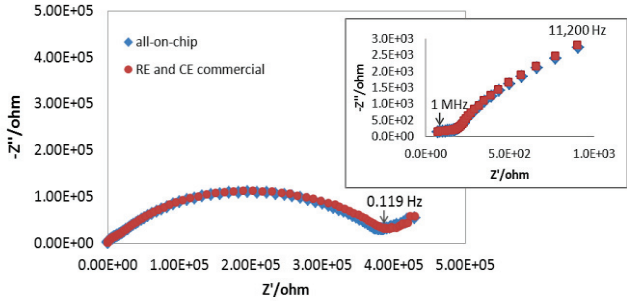

FIGURE 11. Nyquist plot of EIS for D1 microdisc array (N=314, d=100 µm) design using all-on-chip measurement (blue marker) and off-chip RE and CE (red marker) in 1 mM FCA in PBS. $E_{1/2}$ at 0.29 V, frequency 0.01-1MHz (*Inset*: EIS at higher frequency of 11,200 Hz-1MHz).

Typical Nyquist plot for recessed microdisc array was observed for the microdiscs design of D1 and D3 with disc interspacing 100 µm. For the disc interspacing of 50 µm on the other hand, a straight line was noticed in the middle of the real imaginary axis indicating the presence of linear diffusion on the electrode surface resulted from the overlapping diffusion (Fig. 12). For both D1 and D3, linear diffusions at lower frequencies were observed to take place starting from critical frequency 0.119 Hz onwards in both cases. When the interspacing was decreased and the electrodes became more closely packed, these critical frequencies increased to 0.189 Hz and 0.352 Hz respectively

for D4 and D5. These values are in agreement with the scan rate studies where at the more packed array, the linear diffusion took place faster compared to those of largely spaced ones.

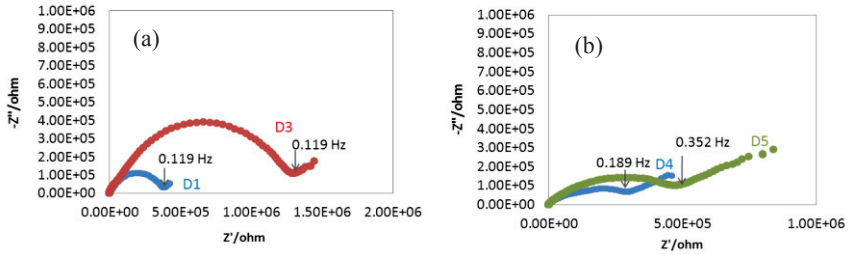

FIGURE 12. EIS spectrum in 1 mM FCA in PBS (frequency 0.01-1 MHz, $E_{1/2}$ at 0.29 V) for (a) D1, N=314 and D3, N=86 (d=100 µm); and (b) D4, N=314 and D5, N=150 (d= 50 µm).

For the microband array, impedance spectra consisted of a semi-circle region followed by a straight line at low frequency. The linear part at the low frequency range implies a mass-transfer limited process and diffusion that still prevail within the recessed band. There was a difference in the semi-circle form and frequency at linear diffusion occurs at the same band array/surface area (Fig. 13a) hence suggesting different diffusion profile to the electrode surface as discussed earlier. For the band array of 18 electrodes reducing the band spacing to half leaded to that the linear diffusion observed at 0.653 Hz, compared to 0.189 Hz, for the 100 µm spacing. The same critical frequences were obtained with a 9 band electrode array. For the B6 however, the impedance was similar to a macroelectrode response where a very small semi-cirle at high frequencies followed by a straight diffusion line (Fig. 13c). This impedance behaviour was in accordance with the suggested diffusion layer (planar diffusion profile).

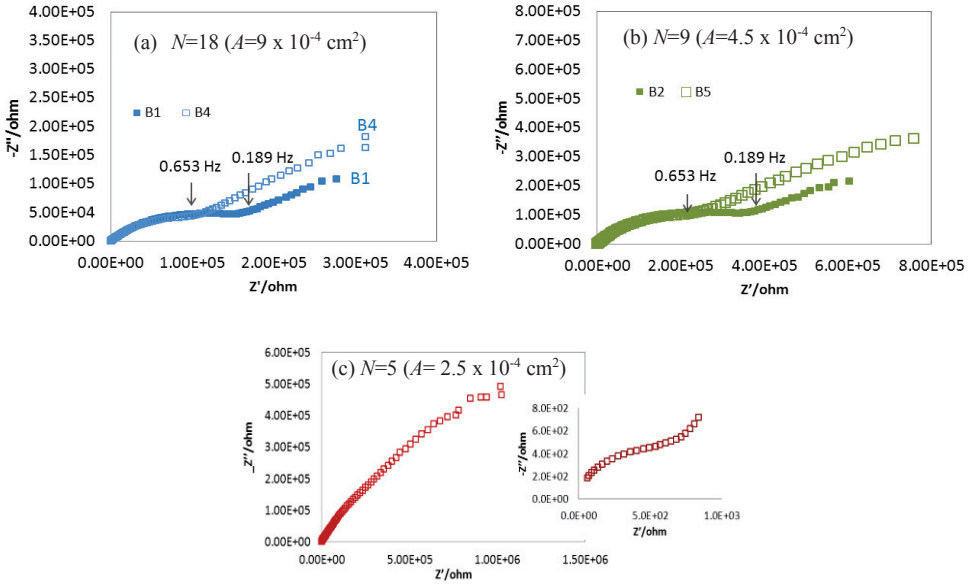

FIGURE 13. EIS spectrum in 1 mM FCA in PBS for the band arrays of same surface area (a) A=9x10^{-4} cm^2 (N=18); (b) A=4.5x10-4 cm2 (N=9); and (c) B6 microband array (N=5, d=50 µm) (*Inset*: EIS at higher frequency of 28,400 Hz -1 MHz). $E_{1/2}$ at 0.29 V, frequency 0.01-1 MHz. Filled marker indicate d=100 µm while non-filled marker indicate d=50 µm.

Based on revealed diffusion profiles the following equivalent circuits can be suggested for the microelectrode arrays. They are: for all disc designs (D1-D6) and B1-B3 as given by Gabrielle et al. [25] which incorporate both spherical impedance (Z_M) and diffusion/Warburg impedance (Z_w) (Fig. 14a); and in the case of B4-B6 where linear diffusion profile was found- the Randles circuit (Fig. 14b) associated with macroelectrode behaviour.

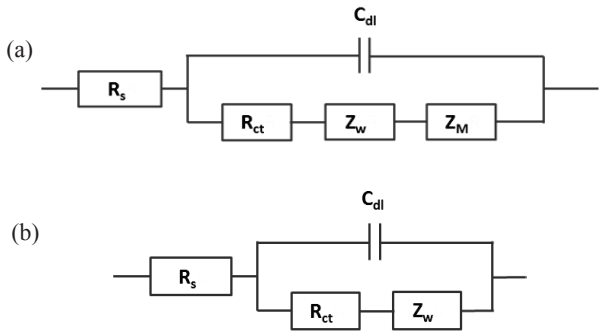

Figure 14: Randles circuit model suggested for (a) microelectrode; and (b) B6 which behaved like a macroelectrode.

CONCLUSION

Overall we can conclude that the design and fabrication of the packageless on-cell microelectrochemical chip which can be used as transducers for different biosensing applications and consists of integrated Pt counter electrode, Ag/AgCl reference electrode and gold microelectrode array of two geometries (band and disc) as working electrode was successful. The electrochemical performance (CVs and impedance spectra) of the on-chip electrochemical cell were the same as for gold on silicon WE with external commercial CE and RE electrodes that approved the adequacy of the design and fabrication process to the application requirements. The performed electrochemical investigation confirmed that the interspacing distance between discs/band in an array (*d*) and radius of the microdiscs (*r*)/width of the band (*w*) are important parameters that influence on the type of electrode diffusion (hemispherical, linear or mixed diffusion profile) and therefore on the shape of the CV and impedance spectra. The experimental results on the limiting currents obtained from CV study were well correlated with the theoretical limiting currents. The shape of impedance spectra corresponded to voltammogram characteristics thus supporting the diffusion behaviour proposed for the different geometries and interspacing distance.

Acknowledgement. The authors gratefully acknowledge the European Commission (FP7 project BOND (Bioelectronic Olfactory Neuron Device), 228685-2) for support of this work.

REFERENCES

1. X. J. Huang, A. M. O'Mahony and R. G. Compton, Small **5**, 776-788 (2009).
2. G. Herzog, W. Moujahid, K. Twomey, C. Lyons and V. I. Ogurtsov, Talanta **116**, 26-32 (2013).
3. W. Moujahid, P. Eichelmann-Daly, J. Strutwolf, V. I. Ogurtsov, G. Herzog and D. W. Arrigan, Electroanalysis **23**, 147-155 (2011).
4. H. Suzuki, Materials Science and Engineering: C **12**, 55-61 (2000).
5. S. Y. Liu, G. Liu, C. Y. Tian, Y. P. Chen, H. Q. Yu and F. Fang, Environmental Science & Technology **41**, 5447-5452 (2007).
6. C. O. Parker, Y. H. Lanyon, M. Manning, D. W. Arrigan and I.E. Tothill, Analytical Chemistry **81**, 5291-5298 (2009).
7. K. Malzahn, J. R. Windmiller, G. Valdés-Ramírez, M. J. Schöning and J. Wang, Analyst **136**, 2912-2917 (2011).
8. K. Twomey, E. A de Eulate, J. Alderman and D. W. M Arrigan, Sensors and Actuators B: Chemical **140**, 532-541 (2009).
9. A. Ahmad and E. Moore, Analyst **137**, 5839-5844 (2012).
10. N. A. M Said, K. Twomey, V. I. Ogurtsov, D. W. Arrigan and G. Herzog, Journal of Physics: Conference Series **307**, 012052 (2011).
11. B. J. Polk, A. Stelzenmuller, G. Mijares, W. MacCrehan and M. Gaitan, Sensors and Actuators B: Chemical **114**, 239-247 (2006).

12. A. Ahmad, “Development of biosensors for the determination of polycyclic aromatic hydrocarbons in environmental monitoring of water,” Ph.D. thesis, University College Cork, Ireland, 2012.
13. Y. P. Chen, Z. Yue, C. Jian, L. Shao-Yang, L. Wen-Wei, L. Gang, T. Yang-Chao, X. Ying and Y. Han-Qing. Electrochimica Acta **55**, 5984-5989 (2010).
14. A. Berduque, Y.H. Lanyon, V. Beni, G. Herzog, Y. E. Watson, K. Rodgers, F. Stam, A. John & Arrigan, D. W. Talanta **71**, 1022-1030 (2007).
15. J. P. Guerrette, S.J. Percival, and B. Zhang, Langmuir **27**, 12218-12225 (2011).
16. A. R. A. Rahman and A. Guiseppi-Elie, Biomedical microdevices **11**, 701-710 (2009).
17. R. B. Morris, D.J. Franta, and H.S. White, The Journal of Physical Chemistry **91**, 3559-3564 (1987).
18. J. Guo and E. Lindner, Analytical Chemistry **81**, 130-138 (2008).
19. D. Menshykau, X. J. Huang, N. V. Rees, F. J Del Campo, F. X. Muñoz and R. G. Compton, Analyst **134**, 343-348 (2009).
20. O. Ordeig, C. E. Banks, T. J. Davies, J. Del Campo, R. Mas, F. X. Muñoz and R. G. Compton, Analyst **131**, 440-445 (2006).
21. G. Schmitt, J-W. Schultze, F. Fassbender, G. Buss, H. Lüth and M. J. Schöning, Electrochimica Acta **44**, 3865-3883 (1999).
22. S. L. Caston and R. L. McCarley, Journal of Electroanalytical Chemistry **529**, 124-134 (2002).
23. D. B. McCreery, W. F. Agnew, T. G. Yuen and L. Bullara, Biomedical Engineering, IEEE Transactions on **37**, 996-1001 (1990).
24. J. D. Weiland, D. J. Anderson, C. C. Pogatchnik and J. J. Boogaard, "Recessed electrodes formed by laser ablation of parylene coated, micromachined silicon probes," in *Engineering in Medicine and Biology Society,* Proceedings of the 19th Annual International Conference of the IEEE Vol. 5 (1997), pp. 2273-2276.
25. C. Gabrielli, M. Keddam, N. Portail, P. Rousseau, H. Takenouti and V. Vivier. The Journal of Physical Chemistry B 110, 20478-20485 (2006).